Soil Biology & Biochemistry 42 (2010) 2254–2265

Contents lists available at ScienceDirect

Soil Biology & Biochemistry

journal homepage: www.elsevier.com/locate/soilbio

Soil heterogeneity effects on O_2 distribution and CH_4 emissions from wetlands: *In situ* and mesocosm studies with planar O_2 optodes and membrane inlet mass spectrometry

Louise Askaer [a], Bo Elberling [a,*], Ronnie N. Glud [b,c,d], Michael Kühl [e,f], Frants R. Lauritsen [g], Hans P. Joensen [a]

[a] Department of Geography and Geology, University of Copenhagen, Øster Voldgade 10, 1350 Copenhagen K, Denmark
[b] The Scottish Association for Marine Science, Dunstaffnage Marine Laboratory, Oban, Argyll, PA37 1QA, UK
[c] Southern Danish University, Institute of Biology and Nordic Center for Earth Evolution (NordCEE), University of Southern Denmark, Odense M, Denmark
[d] Greenland Climate Research Centre, Kivioq 2, Box 570, 3900 Nuuk, Greenland
[e] Marine Biological Laboratory, Department of Biology, University of Copenhagen, Strandpromenaden 5, DK-3000 Helsingør, Denmark
[f] Plant Functional Biology and Climate Change Cluster (C3), University of Technology, Sydney, PO Box 123, Broadway NSW 2007, Australia
[g] Department of Pharmacy and Analytical Chemistry, University of Copenhagen, Universitetsparken 2, 2100 Copenhagen Ø, Denmark

ARTICLE INFO

Article history:
Received 12 July 2010
Received in revised form
12 August 2010
Accepted 23 August 2010
Available online 6 September 2010

Keywords:
Peat soil heterogeneity
Water level
Oxygen availability
Methane
Planar optode
Wetlands

ABSTRACT

The importance of soil heterogeneity for methane emission from a wetland soil is assessed by *in situ* point measurements of depth-specific O_2 and CH_4 concentrations and simultaneous soil CH_4 fluxes at contrasting water levels. Profile measurements, and associated assumptions in their interpretation, were validated in a controlled mesocosm drainage and saturation experiment applying planar O_2 optodes and membrane inlet mass spectrometry. Results show that peat soil is heterogeneous containing dynamic macropore systems created by both macrofauna and flora, which facilitate preferential flow of water, O_2 and CH_4 and vary temporally with changes in the moisture regime. The O_2 content above the water table after drainage varied horizontally from 0 to 100% air saturation within few mm. Oxic zones were observed below the water level and anoxic zones were observed in layers above the water level in periods up to days after changes in the water level. This study shows that although water table position is a competent proxy of soil CH_4 fluxes at larger spatio-temporal scales, it becomes inadequate at higher spatial resolution, i.e. at the scale of the soil pedon and below. High resolution O_2 measurements using planar O_2 optodes have great potential to enhance our understanding of the effect of the water table position on O_2 dynamics on scales of several cm to mm in wetland soils.

1. Introduction

The stability of the wetland carbon pool is sensitive to the availability of molecular oxygen (O_2) and thereby changes in hydrological status (Jobbagy and Jackson, 2000). In general, free O_2 is present above the water table (oxic zone) and is depleted rapidly below it (anoxic zone) primarily due to limited O_2 solubility in water and the $\sim 10^4$ times slower diffusion of O_2 in water as compared to gas (Öquist and Sundh, 1998). However, soil structure and pore geometry play an important role in determining moisture retention and thus determining the extent of oxic and anoxic zones (Weiss et al., 1998). Under anoxic conditions, the decomposition of organic matter involves coupled anaerobic degradation pathways, where CH_4 is the main end product (Le Mer and Roger, 2001). The net effect of marked shifts in water levels on soil O_2 distribution and CH_4 emissions as well as potential feedback mechanisms to global warming remains unclear. An increased understanding of O_2 dynamics in wetlands is thus a prerequisite for a better assessment of present and future CH_4 emissions in responds to potential hydrological changes (IPCC, 2007).

The actual amount of CH_4 emitted to the atmosphere depends on the balance between CH_4 production and consumption as well as the CH_4 transport efficiency (Couwenberg, 2009). Methanotrophic oxidation kinetics is typically an order of magnitude faster than methanogenic production kinetics (Segers, 1998), thus limiting the amount of CH_4 released to the atmosphere. Methane oxidation is mainly confined to a zone close to the water table and

* Corresponding author. Tel.: +45 353 22520, fax: +45 3532 2501.
E-mail address: be@geo.ku.dk (B. Elberling).

0038-0717/$ – see front matter © 2010 Elsevier Ltd. All rights reserved.
doi:10.1016/j.soilbio.2010.08.026

surrounding plant roots, where there is ample O_2 and CH_4 (Dedysh, 2002). However, the transport mode influences the amount of CH_4 available for oxidation. Methane transport is facilitated by diffusion, ebullition and plant-mediated transport, of which the latter two dominate CH_4 transport to the atmosphere (Lai, 2009). Both ebullition and plant-mediated transport allow a direct and rapid transfer of CH_4 across the water–air interface reducing potential methanotrophic consumption. In contrast, CH_4 diffusion plays an important role in supplying methanotrophs in aerobic zones with CH_4 from anaerobic zones (Whalen, 2005).

Previous investigations on the effects of water level change on greenhouse gas emissions from wetlands have shown that high water levels stimulate anaerobic decomposition and CH_4 efflux (Roulet et al., 1993), and the water level is a widely used proxy for CH_4 emission (Couwenberg, 2009). However, some field studies suggest a more complex relationship and poor correlation between net CH_4 emission and the water level status (Wachinger et al., 2000). The direct affect of water level fluctuations on O_2 availability in peat soil and the link between water level and CH_4 dynamics have not previously been investigated in relation to peat structure at a relevant high spatial resolution.

During the last decade planar optodes have provided novel insight on high resolution O_2 dynamics in a range of marine systems such as phototrophic and bioturbated sediments (Fenchel and Glud, 2000; Wenzhöfer and Glud, 2004), rhizospheres (Frediksen and Glud, 2006; Jensen et al., 2005), permeable sand (Precht et al., 2004; Cook et al., 2007) and sea-ice (Rysgaard et al., 2008). However, the technique has only to very limited extent been used in terrestrial or wetland systems (Blossfeld, 2008). The present study i) visualizes and quantifies the O_2 distribution in relation to peat soil structure and water level fluctuations during a controlled drainage and saturation experiment, and ii) relates spatio-temperal variations in O_2 availability to observed soil CH_4 concentrations and emissions both *in situ* and in laboratory mesocosms.

2. Materials and methods

2.1. Study site

In situ measurements and samples for peat mesocosms were collected in a non-managed graminoid (*Phalaris arundinacea*) dominant temperate wetland area, Vedbæk Maglemose, formed through the retreat of an ancient inlet in Vedbæk, Denmark (55°51′N, 12°32′E). The site is located in the temperate zone, where the climate is characterized by a mean annual temperature of 8 °C and a mean annual precipitation of 613 mm (normal for 1961–1990 cf. Danish Meteorological Institute www.dmi.dk). The wetland covers an area of ~0.6 km^2. Peat thickness ranges from 3 m at the deepest points to roughly 0.5 m at the area margins, of which the top 50 cm are terrestrial peat deposits. The wetland surface is ca. 5 m above sea level corresponding to the highest level of the Littorina Sea.

2.2. Sampling and field measurements

2.2.1. Soil analyses

Volume-specific soil samples were taken at 10 cm depth intervals between 0 and 50 cm in 3 replicate bore profiles. Four additional profiles were made within one ha to evaluate the spatial variation within the study area. Values of pH were measured *in situ* (Metrohm 704 Pocket pH meter, Metrohm AG, Switzerland). The soil samples were dried at 60 °C for 3 days to obtain soil bulk density. Total and organic carbon was measured using a CS500-analyser (Eltra GmbH, Germany). Organic carbon was analyzed after removal of inorganic carbon using 3 M HCl. Standard deviations of replicates of total carbon were <5%.

Peat core samples from 4 depths between 0 and 50 cm below the surface, representing distinct peat layers, were prepared for solid-state ^{13}C NMR analysis. Samples were freeze-dried and milled. Solid-state ^{13}C NMR spectra were obtained using a Bruker DSX 200 (Bruker, Germany) NMR machine operating at a frequency of 50.3 MHz using zirconium rotors of 7 mm OD with KEL-F-caps. The CPMAS technique (Schaefer and Stejskal, 1976) was applied during magic-angle spinning of the rotor at 6.8 kHz. A contact time of 1 ms was used for all spectra. The ^{13}C-chemical shifts were calibrated to tetramethylsilane (TMS) (=0 ppm) and were calibrated with glycine (176.04 ppm). Between 7951 and 169,040 single scans were made for each spectrum. Line broadening of 50.00 Hz was used. The relative intensity of the peaks was obtained by integration of the specific chemical shift ranges by an integration routine supplied with the instrument software. The relative intensity of O/N-alkyl C was used as an indicator of the lability of the carbon fraction at different depths. Flowers and seeds of terrestrial plants (e.g. *Chenopodium*) and shells of marine snails (e.g. *Hydrobia ventrosa*) were selected for AMS ^{14}C measurements from 6 depths intervals within the upper 30 cm. The macrofossils were dried at 70 °C and treated with 1% HCl and 0.5% NaOH before ^{14}C analysis.

Basal soil respiration rates were measured in the laboratory using bulk soil samples from 2, 5, 10, 20 and 40 cm depth. Soil samples were transferred to 12-ml Venoject tubes (Terumo, Europe, N.V.), preincubated for 2 h and out-gassed with CO_2-free air for 5 min. Soil respiration was subsequently measured using gas chromatography by monitoring the linear increase of headspace CO_2 concentrations ($r^2 > 0.9$), using a GC (ML-GC8212, Micro-Lab, Bozeman, MT, USA) equipped with a Porapak Q column kept at 30 °C and a thermal conductivity detector (Mikrolab Aarhus A/S, Denmark). All measurements were made at a constant room temperature of 20 °C.

2.2.2. Soil CH_4 emission measurements with closed static flux chambers

Three replicate PVC collars with 110 mm inner diameter were installed to a depth of 8 cm leaving 2 cm above the soil surface. During measurements a closed chamber was made using a closed-end stainless steel CHA Type coupling as a lid which could be securely fitted on the base collars. The total volume of the chamber averaged 0.5 L. Before the lid was attached to the base collar, a gas sample was taken in the centre of the base collar. Subsequently, chamber headspace samples were extracted three times at 15 min intervals. Samples were taken in a plastic syringe and injected into a 2.5 ml glass injection flask with an 11 mm collar; flasks were closed with a septa lid consisting of polyisobutylene rubber fitted to the injection flask with an 11 mm aluminium capsule using a tong (Mikrolab Aarhus A/S, Denmark). Samples were analyzed within 24 h using a Shimadzu GC 2014 (Japan) equipped with a back flush system with a Mol Sieve 5A 80/100 mesh (1/8″ × 1 m) column connected to an FID detector.

As samples were extracted by syringe, compensation air was simultaneously drawn into the chamber through a 10 cm long (1 mm id) pressure equilibrium tube. The sample withdrawal was ~4% of the total air in the chamber. Before each measurement, the chamber air was mixed. Soil temperatures at 5 cm depth were measured simultaneously at each of the 3 replicate chambers. Soil CH_4 fluxes were measured weekly and during targeted field campaigns the O_2 and CH_4 concentration profiles were measured concurrently.

2.2.3. Depth-specific gas sampling – silicone probes

Air in the soil pores was sampled for CH_4 analyses at depths 5, 10, 20, 30, 40, 50, 60, 80, 110 and 140 cm using probes constructed from silicone tubing as described by Kammann et al. (2001). Each probe consisted of 1.3 m of tubing (id 10 mm, wall thickness 3 mm, total probe volume 100 ml) closed with rubber septa at both ends.

The tubing was rolled into a coil and fixed by steel wire. A 0.92 mm (id) stainless steel tube was inserted through the outer septa of the probe to connect the silicone probe in the soil with the soil surface (1 ml dead volume per meter steel tube). The end of the steel tube was fitted with a three-way stopcock to enable the soil air to be sampled undisturbed from the soil surface. The probes were installed by pre-cutting a 20 cm × 3 cm semicircular cavity in a soil pit wall. Probes were inserted into each cavity and the soil was noted to collapse around the probe after insertion. The pit was refilled with soil, horizon by horizon. Soil gas samples were taken with 60 ml plastic syringes and transferred to the same injection flasks using the same procedure, and analyzed at the same laboratory, as gas samples from the static chambers (see above). Roughly 40 ml of gas sample was withdrawn from each probe.

2.2.4. Oxygen sensors

The O_2 content was measured *in situ* with an optical O_2 sensor array (Rickelt et al., in preparation) at 5, 10, 15, 20, 30, 40, 50, 60, 80 and 120 cm depth. Ten O_2 optodes (Kühl, 2005) were mounted into a PVC soil spear, which was inserted in the peat soil. Each sensor consisted of a robust fibre-optic O_2 optode mounted together with a type K mini thermocouple enabling temperature compensated measurements. The O_2 optodes were connected to a multichannel fibre-optic oxygen meter (FIBOX-4 or FIBOX 10, Presens GmbH, Germany) and the thermocouples were connected to a thermocouple thermometer (RS 206-3722, RS Components Ltd., Taiwan). All sensors were calibrated by a 2 point temperature and O_2 calibration. Sensors measured with a standard deviation $\leq$5% and an average 90% response time across the measuring range (0–100% air sat.) of ~15 min.

2.2.5. Water level

Soil water level was monitored in a 2.5 m long perforated plastic tube. Water level depths were measured manually simultaneously with static chamber CH_4 sampling and soil O_2 content measurements.

2.3. Laboratory experiments

2.3.1. Experimental setup

Mesocosm peat core samples were taken in three semicircular PVC columns (id: 20 cm *H*: 60 cm), mounted with a 8 cm wide planar plexiglas sheet on which the planar O_2 optode was fixed (Fig. 1) using a thin film of distilled water and fastening the edges with black tape. Peat cores, 20 cm in diameter and 55 cm in height were collected from the field using a three-stage extraction procedure according to Freeman et al. (1992) to avoid compaction. Cores were taken during winter to obtain dormant vegetation and high water level. After extraction the peat columns were insulated and kept in the dark to eliminate plant photosynthesis and avoid development of microphytes along the planar optode. Cores were moved into a dark climate chamber kept at 10 °C and water levels were adjusted to 5 cm above the soil surface in all cores. The cores were preincubated for 1 month to obtain steady state conditions with respect to O_2 and CH_4. A water-saturated soil disc (Prenart Equipment Aps, Denmark), soil water sampler (porous PTFE/quartz) was inserted in the bottom of the column. The column was hermetically closed from below by two aluminium sheets (3 mm thick) with rubber coating. A large opening was made in a similar top sheet for the membrane inlet mass spectrometer (MIMS) (Section 2.3.3).

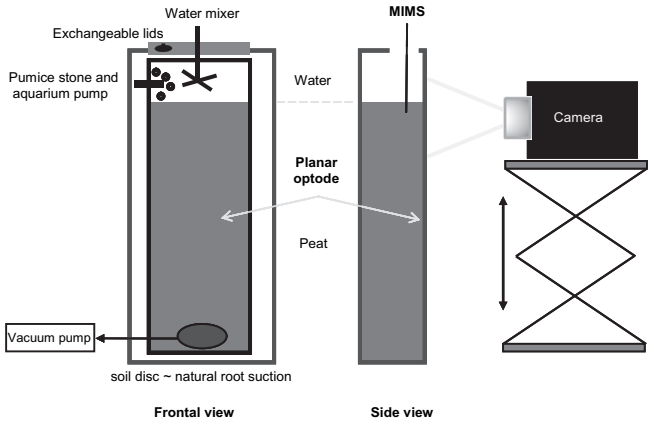

Fig. 1. Schematic drawing of the experimental setup for monitoring O_2 dynamics in peat soil mesocosms by a planar optode imaging system (not to scale).

One type of lid was made holding the water mixer and an opening for pressure equilibrium. Another type of lid was made gastight and equipped with a septum for headspace sampling. The initial water level was maintained 5 cm above the peat surface. An aquarium pump and pumice stone was used to maintain constant O_2 concentrations in the water and a water mixer, rotating 5 times per minute ensured constant O_2 concentrations throughout the water column. To ensure constant atmospheric O_2 concentrations above the peat core during drainage periods, water-saturated air was continuously circulated through the top of the PVC column.

Steady state conditions were confirmed during the last week of preincubation by daily gas profiling using the MIMS and planar O_2 optode imaging.

Drainage and saturation experiments were performed to simulate the effect of water level changes induced by evapo-transpiration and natural rainfall on O_2 concentrations and consumption rates in the peat soil. To study the rate of O_2 transport into peat soil during drainage, a suction of 300 mbar was applied to the soil disc, representing natural root suction until water levels reached −40 cm after 2 days. To quantify effects of flooding, soil water was carefully added to the peat soil surface over styrofoam to avoid damages to the peat surface structure. Water was continuously added over 10 h until the water level was stable at +5 cm above the peat soil surface. For measuring of water level movements, a perforated tube with a sealed bottom was inserted and the water level in relation to the sediment surface was measured over the duration of drainage and saturation. During changes in water level, planar O_2 optode images were taken at 10 min intervals to study the spatio-temporal dynamics of O_2 in the peat profile. MIMS-based measurements of CH_4 concentrations (see below) at 4 cm depth were made simultaneously at 10 min intervals during the drainage sequence.

2.3.2. Oxygen planar optode

The applied planar optode measuring setup for 2-D O_2 measurements has been described in detail by Glud et al. (1996) and Holst et al. (1998, 2002). As for other O_2 optodes systems the basic principle of the planar optode is the ability of O_2 to act as a dynamic quencher of the luminescence intensity of an immobilized O_2 indicator (recently reviewed in Kühl and Polerecky, 2008). Here we used the O_2 quenchable indicator dye Ruthenium(II)-tris-4,7-diphenyl-1,10-phenanthroline (Ru-dpp) immobilized in a ~20 μm thick polystyrene layer cast onto a 0.125 mm-thick transparent polyethylene terephthalate carrier foil (Mylar, Goodfellow, UK). The indicator is excited by blue light (ex. max. 460 nm) inducing red luminescence (em. max. 610 nm), which is quenched in the presence of O_2. Two planar optode foils (100 × 250 mm) were taped together (100 × 500 mm) and mounted on the inside of a plexiglass sheet glued onto the cut PVC cylinder (section 2.3.1).

In the experimental setup, excitation light was supplied by an array of blue light-emitting diodes (LED) ($\lambda = 470$ nm) illuminating the sensor foil from behind through the Plexiglas and the Mylar foil. Images of the O_2 dependent luminescence were obtained with a thermoelectrically cooled gate-able charge coupled device (CCD) camera (SensiCam Sensimod, PCO Computer Optics, Germany) equipped with a 25 mm/1.4 Nikon wide-angle lens. All O_2 images were obtained without ambient light.

The camera and LED's were part of a modular luminescence lifetime imaging system (MOLLI) for image acquisition and processing (see details in Holst et al., 1998). A "by area average" two-point calibration was performed at 100% and 0% air saturation to enable image calibrations using a modified Stern–Volmer equation (Klimant et al., 1995). The obtained O_2 images covered an area of 70×50 mm (CCD camera chip size 640×480 pixel). More details about optical O_2 imaging, sensor materials, measuring and calibration routines are given elsewhere (Glud et al., 1996, 2001; Holst et al., 1998, 2002; Kühl and Polerecky, 2008).

2.3.3. Membrane inlet mass spectrometry (MIMS)

Depth-specific analyses of dissolved CH_4 concentrations were carried out using a MIMS similar to that developed by Lloyd et al. (Bernstead and Lloyd, 1994; Thomas and Lloyd, 1995; Lloyd et al., 1996; Cowie and Lloyd, 1999) and a detailed description of the method and the MIMS probe itself is found in Sheppard and Lloyd (2002). Our probe was a 50 cm long stainless steel probe (3.2 mm o.d, 1.6 mm i.d.) fitted with a 20 mm long narrow tip (1.6 o.d., 1.0 mm i.d) in one end and attached to the mass spectrometer at the other end via a 50 cm long flexible metal bellow. The narrow tip was closed in the end and had a 0.5 mm orifice drilled 1 cm from the end. The orifice was covered with a 50 μm thick microporous polypropylene membrane (CELGARD 2502, Hoechst Celanese, Charlotte, NC) with an effective pore size of 0.075 μm and a porosity of 45%. In contrast to the silicone rubber membranes used by Lloyd et al. (1996), this type of membrane does not result in a highly preferential transport of gases as compared to water through the membrane; instead all compounds pass the membrane at a comparable rate (Lauritsen et al., 1992). The missing enrichment of gases as compared to water is compensated by a 50–100 times higher flux of water and gas through the membrane into the probe and the mass spectrometer. With the membrane probe inserted in water a total pressure inside the mass spectrometer below 1×10^{-5} torr is obtained, which corresponds to a maximal liquid (water and gases) consumption rate of 1 nL/s for our mass spectrometer system. The mass spectrometer was a quadrupole mass spectrometer (QMA 125, Balzers, Lichtenstein).

2.3.4. Headspace gas measurements

Headspace gas was sampled at 15 min intervals for a period of 45 min. Samples were taken and analyzed as described for the field measurements (section 2.2.2). The sample withdrawal was ~1% of the total air in the chamber. Before each measurement, the chamber air was mixed carefully by slowly pumping 5 ml (0.25% of total sample) air out of the chamber and into the chamber again using the syringe.

2.4. Analytical procedures

Headspace measurements from the static chambers and mesocosms were used to calculate gas fluxes (Fc) by equation (1):

$$Fc = \frac{(\Delta C/\Delta t)Vp}{RTA} \quad (1)$$

where ΔC is the change in concentration in ppm, Δt is the measurement period in seconds, V is the volume of air in the chamber in m^3, p is the atmospheric pressure during measurement time in atm., R is the ideal gas constant in m^3 atm mol^{-1} K^{-1}, T is the temperature in the chamber in Kelvin and A is the basal area of the chamber in m^2. $(\Delta C/\Delta t)$ was determined by linear regression on concentration vs. time measurement. Only 4 samples were taken, yielding a low degree of freedom, therefore a significance test was made to remove measurement series where $p > 0.25$.

The diffusive oxygen flux into the soil across the soil surface (μmol m^{-2} h^{-1}) was calculated from a modified Fick's first law of diffusion:

$$\mathrm{DOU} = \frac{(D_o)\mathrm{d}C}{\mathrm{d}z} \quad (2)$$

where DOU is the diffusive oxygen uptake, D_o is the molecular diffusion coefficient for O_2 in water at the given temperature (1.44×10^{-5} m^2 h^{-1} at 10 °C cf. Wilke and Chang, 1955) and dC is the change in O_2 content (mmol m^{-3}) over a depth interval, dz (m) measured across the diffusion boundary layer immediately above the soil–water interface. The mean O_2 consumption rate below the soil–water interface (m^3 h^{-1}) was estimated as DOU divided by the O_2 penetration depth (m). Throughout the paper mean values are given with 1 standard deviation from the mean (±1 SD).

3. Results

3.1. Soil characteristics

The organic material in the top 0.5 m of the peat soil was deposited in a freshwater lake subsequently turning into a moist wetland (Christensen, 1981). ^{14}C dated macrofossils showed that the top 30 cm were deposited within the last 40 years resulting in an average peat accumulation rate of 11.4 mm yr^{-1}. The peat deposited organic carbon (0–30 cm depth) amounted to 29 kg m^{-3} thereby resulting in a mean accumulation rate of 730 g C m^{-2} yr^{-1} (Fig. 2a). The soil profile could be divided into three main layers: surface 10 cm, the 10–30 cm and 30–50 cm depth horizons.

The surface layer (top 10 cm) accumulated within the past 20 years and exhibited a bulk density from 0.25 g cm^{-3} this value gradually increased to 0.41 g cm^{-3} at 40 cm depth (Fig. 2a). The mean pH and SOC content in the surface layer were pH 7.3 and 28%, respectively. In deeper layers, pH generally decreased with depth to pH 7.0 and SOC increased slightly reaching a maximum of 31.6 ± 7.7% at 40 cm depth, although not differing significantly from concentrations above (Fig. 2b–c). Basal soil respiration (BSR) and O/N-alkyl C intensity were 20 μg C g SOC^{-1} h^{-1} and 50, respectively, in the soil surface and decreased markedly to 10 and 38 μg C g SOC^{-1} h^{-1}, respectively, within the top 10 cm (Fig. 2d). Below 10 cm depth, BSR remained relatively constant at 10 μg C g SOC^{-1} h^{-1} down to 50 cm depth. The O/N-alkyl C intensity decreased steadily throughout the soil profile reaching 30% at 50 cm depth.

3.2. Field observations

3.2.1. Oxygen and methane concentrations at 3 contrasting water levels

Field measurements of depth-specific soil CH_4 and O_2 concentrations and simultaneously measured soil CH_4 fluxes at three contrasting water levels, i.e. water table 2.2, 17.7 and 49.8 cm below the soil surface, were done on 09.05.09, 03.05.09 and 07.06.09, respectively (Fig. 3a–c). Soil surface temperatures (5 cm) at these dates were 11.7 ± 0.7 °C, 10.6 ± 0.8 °C and 12.7 ± 0.9 °C, respectively. At all 3 dates, the O_2 content below the water table was <2% air saturation. Above the water table, the O_2 content differed dependent on the actual depth below the soil surface. When the

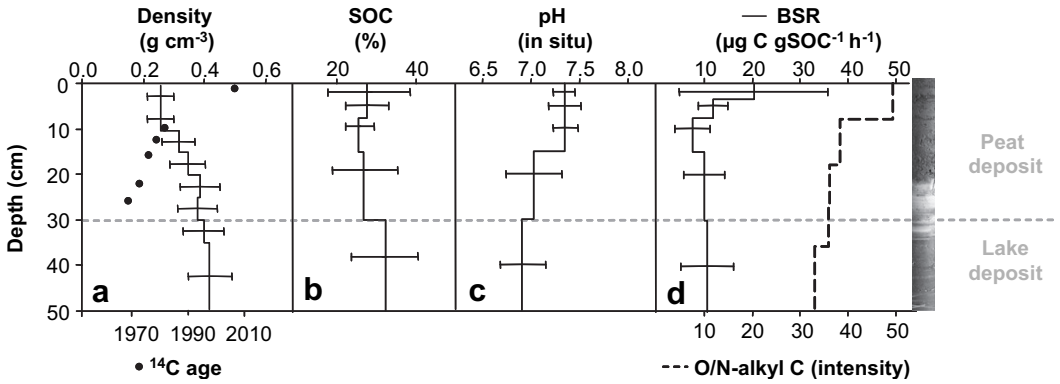

Fig. 2. Depth-specific soil properties. SOC: soil organic carbon. BSR: basal soil respiration. O/N-alkyl C is the most labile carbon compound in the soil substrate and can therefore be used as a measure of the stage of decomposition and soil reactivity. Horizontal perforated lines indicate change of depositional environment. Error bars show 1 standard deviation from the mean, $n = 3$.

water level was at 17.7 cm below the soil surface (Fig. 3b) the O_2 content was 78% air sat. at 5 cm depth. At 10 and 15 cm depth the oxygen content was <2%. At a water level depth of 49.8 cm below the soil surface, the O_2 content decreased from 97% air saturation at 5 cm depth to 68% air saturation at 20 cm depth. The O_2 content from 25 to 40 cm depth were between 2 and 5% air saturation.

CH_4 concentrations increased with depth below the water table and decreased with distance above the water table in all situations. Soil CH_4 concentrations varied with the depth of the water table. The soil CH_4 concentration at 5 cm depth was 107 ppm when the soil was fully water saturated in contrast to 22 and 11 ppm when the water level was −17.7 and −49.8 cm respectively. When the water level was at −2.2 cm depth, the soil CH_4 concentration rose 10-fold at 10 cm depth until it reached a stable concentration of ca. 3,500 ppm down to a depth of 60 cm where concentrations increased to ca. 15,000 ppm. When the water level was at −17.7 cm depth soil concentrations of CH_4 were stable at ca. 20 ppm above the water level and rose to ca. 4200 ppm just below the water level. From 20 to 60 cm depth, CH_4 concentrations remained relatively stable at ca. 3500 ppm before increasing to ca. 15,000 ppm in deeper layers. When the water level was at −49.8 cm depth, the lowest soil CH_4 concentrations were measured at the soil surface (5–20 cm depth). At 40 cm depth the CH_4 concentration had increased to 121 ppm and just below the water level the CH_4 concentration was found to increase rapidly to ca. 8000 ppm at 50–60 cm, 14,000 ppm at 80 cm, 21,000 ppm at 110 cm and 35,000 ppm at 140 cm respectively.

3.2.2. Soil methane flux vs. water level

Soil CH_4 fluxes at the three contrasting water levels differed (Fig. 3a–c). During the period of near-surface water level (−2 cm), a net soil CH_4 efflux of 0.13 ± 0.1 mg CH_4-C m^{-2} d^{-1} was measured. When the water table was 18 cm below the surface, a net CH_4 soil uptake was observed (-0.13 ± 0.12 mg CH_4-C m^{-2} d^{-1}). When the water level decreased to −50 cm the measured soil CH_4 uptake increased to -0.22 ± -0.05 mg CH_4-C m^{-2} d^{-1}. Atmospheric CH_4 concentrations immediately above the soil surface (T_0) also differed significantly dependent on the soil CH_4 flux ($n = 3$, $p = 0.003$). At a high water level (−2 cm) and subsequent CH_4 emissions the T_0 concentration was 2.32 ± 0.04 ppm whereas at a low water level

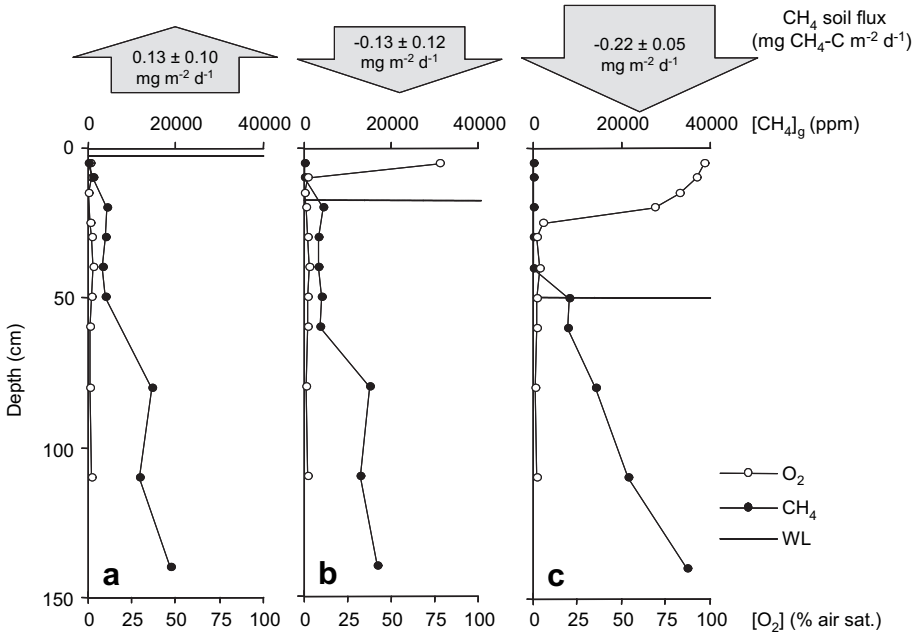

Fig. 3. Field measurements of depth-specific O_2 and CH_4 concentrations and CH_4 soil fluxes at three dates with contrasting water levels. a) WL: −2.2 cm on 09.05.09, b) WL: −17.7 cm on 02.05.09, c) WL: −49.8 cm on 07.06.09.

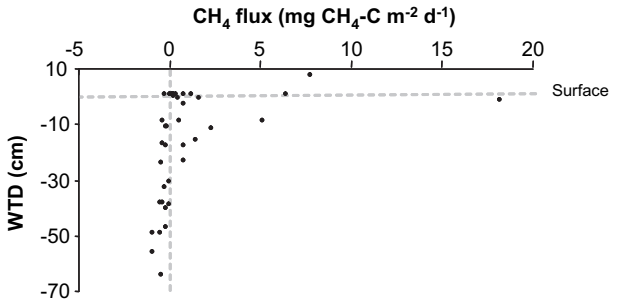

Fig. 4. Weekly static chamber CH_4 flux measurements plotted against water level (cm below soil surface). Horizontal perforated line indicates peat surface. Vertical perforated line indicates the boundary from soil CH_4 uptake to soil emission. (Linear best fit: $y = 1982.2x - 19.5$, $r^2 = 0.11$).

(−50 cm) and subsequent net soil CH_4 uptake the T_0 concentration was 1.75 ± 0.1 ppm. Weekly measurements of soil CH_4 fluxes showed a shift from net release to net uptake when the water level dropped below −30 cm (Fig. 4).

3.3. Experimental observations

3.3.1. Oxygen and methane concentrations in the waterlogged peat soil

Two-dimensional mapping of O_2 in the saturated peat soil showed the presence of a relatively uniform O_2 penetration depth of 4.6 ± 0.2 mm ($n = 3$) following the soil contours (Fig. 5a–c, Table 1). Below this depth, the O_2 content was below the detection limit (Fig. 5c). The DOU was calculated to 864 ± 173 μmol O_2 m^{-2} h^{-1} ($n = 3$) (Eq. (2)) resulting in a mean volume-specific O_2 consumption in the soil–water interface of 5.2 ± 1.0 nmol O_2 cm^{-3} s^{-1} ($n = 3$).

Three MIMS CH_4 profiles were made on different dates on the same waterlogged peat column (Fig. 5a), and the exhibited the same overall pattern although absolute concentrations differed markedly (Fig. 5a). Lowest CH_4 concentrations were measured near the surface in the oxic zone and down to a depth of 1 cm. CH_4 concentrations were found to increase to a maximum concentration at ~5 cm depth where concentrations ranged from 365 to 546 μM. Concentrations decreased to between 175 and 186 μM 25 cm depth. Between 25 and 40 cm depth, CH_4 concentrations increased to concentrations close to the maximum concentrations found at 5 cm depth. After profiling with the MIMS, ebullition of gas was observed from the hole produced. Average headspace measurements of CH_4 emissions from the fully saturated peat soil was 65.4 ± 103.7 mg CH_4-C m^{-2} d^{-1} ($n = 3$) of which one of the mesocosm emissions differed significantly from the other two, possibly due to CH_4 ebullition resulting in the large SD. Ignoring the mesocosm with the high emission rate gave an average emission rate of 0.18 ± 0.01 mg CH_4-C m^{-2} d^{-1} which was similar to emissions measured in the field at similar environmental conditions (fully water saturated, 10 °C).

Table 1
Oxygen characteristics of the fully saturated peat soil at the soil–water interface ± 1 standard deviation. Average volume-specific O_2 consumption measured in the soil–water interface. $n = 3$.

O_2 penetration depth (mm)	4.6 ± 0.2
Diffusive oxygen uptake (μmol O_2 m^{-2} h^{-1})	864 ± 173
Average volume-specific oxygen consumption (nmol O_2 cm^{-3} s^{-1})	5.2 ± 1.0

3.3.2. Oxygen and methane dynamics during drainage

During the drainage sequence, the O_2 content in the peat soil increased from 0% air saturation to 55% air saturation within 42 h (Fig. 6a, b). As the water level decreased below the surface, compaction of the swelled peat was observed on the planar optode image (Fig. 6a $T_{30} - T_{1400}$). The O_2 penetration followed a preferential flow pattern through macropores resulting in a heterogeneous O_2 distribution. As the water level dropped from 0 cm to −12 cm, the O_2 content at 4 cm depth increased from 3 to 25% air saturation while CH_4 concentrations at 4 cm depth were constant around 600 μM (Fig. 6b). Soil CH_4 concentrations decreased when the soil O_2 content on average increased above 30% air saturation. As the water level further decreased to −20 cm depth from 1400 to 1750 min, O_2 content increased to 34% air saturation and CH_4 concentrations decreased from the stable concentration of 600 μM to roughly 500 μM at 1750 min. Between 1750 and 2020 min the water level decreased to −26 cm. The O_2 content increased only slightly to 35% air saturation yet the CH_4 concentration decreased from 500 μM to 150 μM. Penetration of O_2 followed soil macropores and although the water table was well below the height of the planar optode image there were both oxic and anoxic zones within the soil depth studied (Fig. 6). After

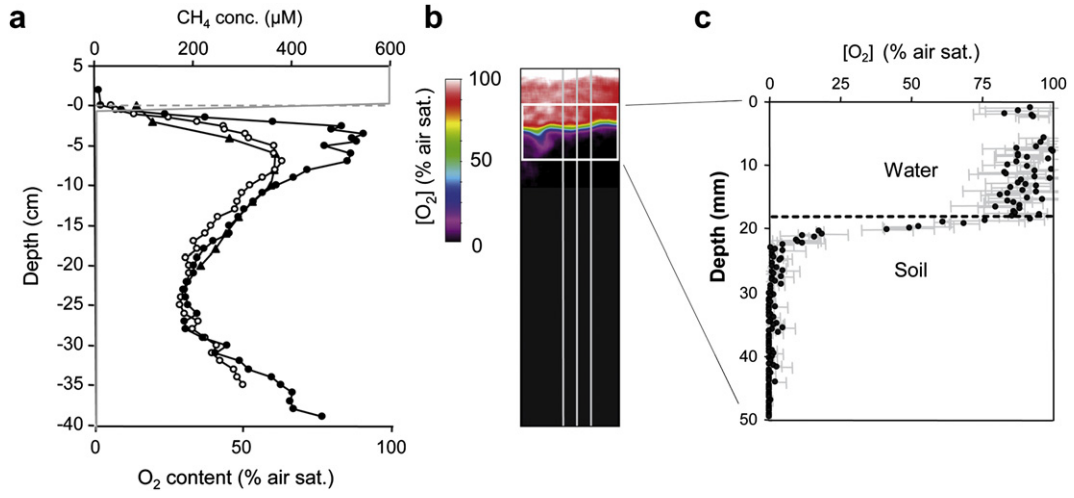

Fig. 5. (a) Three depth profiles of CH_4 concentrations (μM) and O_2 content (air sat.) in a soil mesocosm on three dates (▲ 29.11.07, ○ 30.11.07, ● 03.12.07). CH_4 concentrations profiles are measured by membrane inlet mass spectrometry. The O_2 profile is an average of the three profiles shown in the planar optode image (b). (c) The average O_2 content from three profile lines in the soil–water interface (marked by a box in image (b)) including 1 SD from the mean.

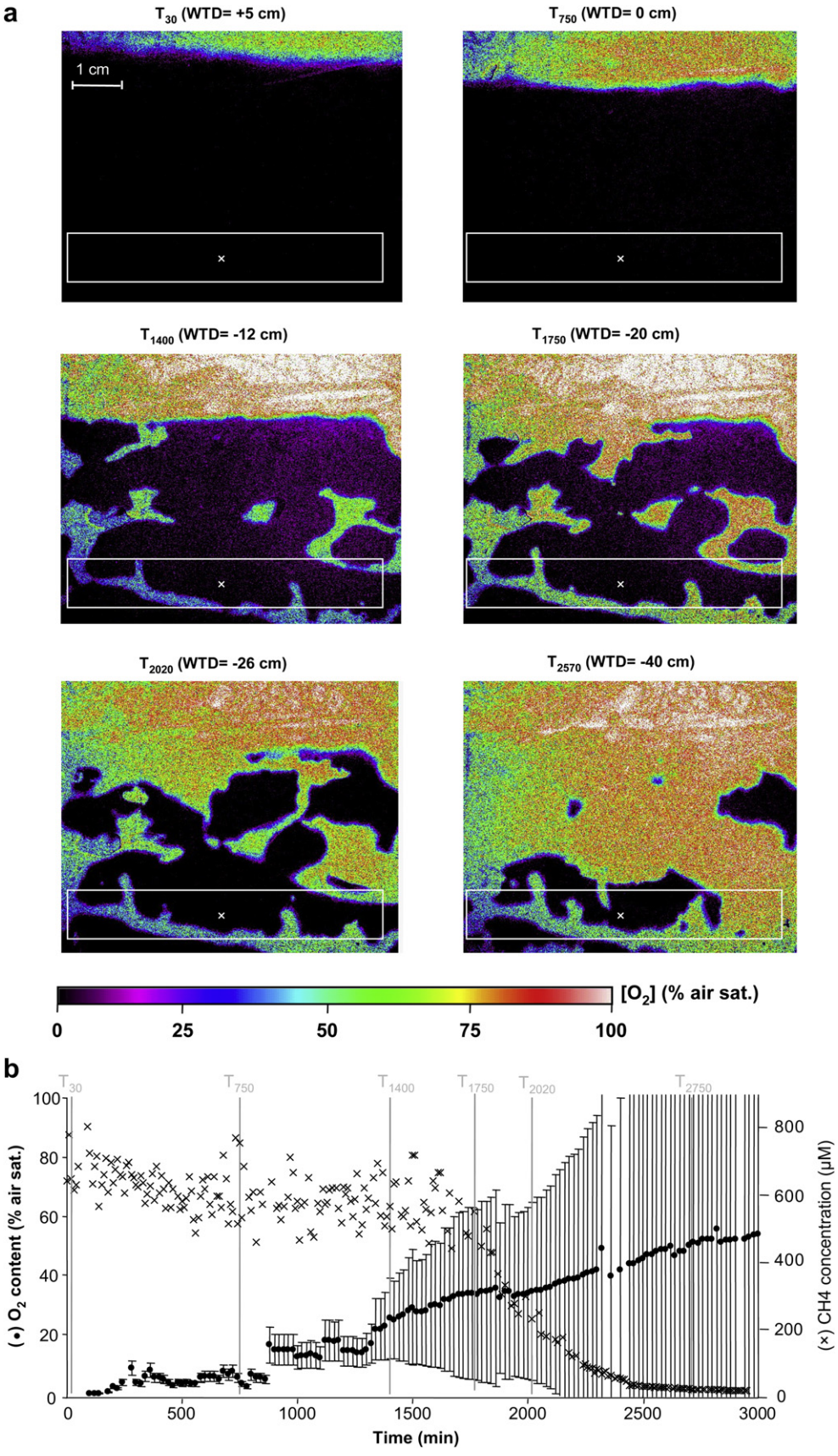
a
T30 (WTD= +5 cm)
T750 (WTD= 0 cm)
1 cm
T1400 (WTD= -12 cm)
T1750 (WTD= -20 cm)
T2020 (WTD= -26 cm)
T2570 (WTD= -40 cm)
[O2] (% air sat.)
0
25
50
75
100
b
T30
T750
T1400
T1750
T2020
T2750
(•) O2 content (% air sat.)
(×) CH4 concentration (µM)
Time (min)
0
500
1000
1500
2000
2500
3000
0
20
40
60
80
100
0
200
400
600
800

2750 min the water level was at −40 cm and the O_2 content was 49% air saturation and the soil CH_4 concentration was below 25 μM. As the O_2 saturation increased further to above 55% air saturation, the soil CH_4 concentration decreased below 10 μM. The standard deviation of O_2 measurements differed considerably dependent on the point of time in the drainage sequence. During fully water-saturated conditions where the soil was anoxic standard deviations ranged from 0 to 5% air saturation whereas during drainage the heterogeneity of O_2 level increased immensely with standard deviation increased to 100%. After prolonged drainage, standard deviations decreased as soil O_2 content became more homogeneous. The planar O_2 optode images of the drainage sequence covering a period of 50 h (at a frame rate of 10 min intervals), has been combined to a short movie visualizing the O_2 availability during a drainage sequence (Supporting information, Video 1).

3.3.3. Oxygen dynamics during saturation

During water saturation, the mean O_2 image content (12 cm^2) decreased from 57 ± 16% air saturation to <1% air saturation within 22 h (Fig. 7a, b). The water followed preferential flow patterns as water first filled the soil macropores. From O_2 measurements at 10 min intervals, it was observed that O_2 contents declined most rapidly within the first 10 min after saturation (0.16 μmol O_2 cm^{-3} s^{-1}). Within the first hour after water saturation, the O_2 depletion rate decreased to 0.12 μmol O_2 cm^{-3} s^{-1} and between 330 and 1330 min after water saturation O_2 depletion rates decreased to 0.01 O_2 μmol cm^{-3} s^{-1}. From 22 to 50 h after water saturation, O_2 depletion rates decreased to 0.001 μmol O_2 cm^{-3} s^{-1}, i.e. the same magnitude as O_2 consumption in the soil–water interface. An oxic soil aggregate (O_2 content >10% air saturation) was present at the 3 cm depth up to 24 h after the saturation event. The volume-specific O_2 consumption rate within this aggregate was calculated to be ca. 0.045 nmol O_2 cm^{-3} s^{-1}, considerably slower than in the surrounding soil. The planar optode measurements showed a large heterogeneity in the soil O_2 availability. As the soil became more saturated and the O_2 content decreased, standard deviations also decreased. The planar O_2 optode images of the saturation sequence (10 min intervals) were combined to a short movie visualizing the O_2 depletion during drainage (Supporting information, Video 2).

3.3.4. Heterogeneity of peat O_2 distribution – impact of bioturbation

The drainage and saturation sequence showed a biotic controlled heterogeneous soil structure resulting in small-scale variations in the O_2 availability (supporting information, Videos 1–3). During drainage, preferential flow of water and O_2 was observed along worm borrows and grass stalks resulting in O_2 contents ranging from as low as 0% to 100% air saturation well above the water level (Fig. 8a–c). Video 3 (Supporting information, Video 3) shows the effect of bioturbation before and under drainage, where macrofauna including earthworms move in the soil creating first a pathway where O_2 contents are lower around the worm that subsequently acted as a macropore with a faster response to changes in O_2 supply. Overall, the two-dimensional O_2 imaging performed during the drainage and saturation showed a highly dynamic subsurface O_2 distribution that cannot with the same spatial resolution be portrayed by point measuring probes.

4. Discussion

4.1. Soil characteristics

The spatial distribution of labile C is a key aspect of the potential effects of changes in water level on subsurface C dynamics. We used ^{13}C NMR to identify functional C compounds, relative reactivity, and their spatial variation within the soil profile. The surface peat contained a high amount of labile O/N-alkyl C indicative of high soil degradability (Kiem et al., 2000). This is in line with the observed high basal soil respiration rates in the same depths (Fig. 2d) and the young age of organic material deposited in the surface layers. The high accumulation rate of organic carbon in our site is considered due to a large biomass of *P. arundinacea* produced annually (Landström et al., 1996). The high reactivity of the soil surface layer suggests that labile substrate is not a limiting factor for CH_4 production under anaerobic conditions. While the presence of O_2 is the most important constraint on methanogenesis in wetlands, previous laboratory studies indicated that substrate supply is the primary control once anaerobic conditions have been achieved (Whalen, 2005). This implies that substrate may be a limiting factor in deeper layers.

4.2. Soil O_2 and methane concentrations

Soil CH_4 concentration profiles at three contrasting water levels (Fig. 3) showed that O_2 availability is closely related to the water level and limited by the low O_2 solubility and diffusion in water as compared to air. Few mm below the water level the soil was anoxic containing O_2 contents below the detection limit (Fig. 6a). The actual depth of the water level below the soil surface also affects the distribution of O_2. Above the water level, the moisture content and the corresponding diffusivity is strongly influenced by capillary rise and the high water holding capacity of peat (Witkowska-Walczak et al., 2002; Weiss et al., 1998). This was seen in the planar optode images during the drainage sequence (Supporting information, Video 1). Therefore O_2 contents do not increase substantially in close vicinity to the water level and therefore, anoxic conditions were noted 10–30 cm above the actual water level.

Soil CH_4 fluxes were directly influenced by the water level, when the water level fluctuated between 0 and 30 cm. When water levels dropped below −30 cm, the soil CH_4 efflux ceased, during such conditions all the produced CH_4 was apparently oxidized within the soil matrix before reaching the soil surface. This is consistent with other studies showing a rapid CH_4 oxidation by methanotrophs in the presence of O_2 (Watson et al., 1997).

Gas transport mechanisms driven by pressure gradients transport CH_4 away from anoxic aggregates (Thorstenson and Pollock, 1989) The anoxic zones present above the water level (Fig. 6) facilitate CH_4 production but were apparently not large enough to exceed the CH_4 oxidation at the interface between such anoxic microenvironments and oxic surroundings. This is observed as there is an immediate decrease in CH_4 concentrations above the water level despite the anoxic zones. Higher concentrations of CH_4 (up to 35,000 ppm) observed below 50 cm depth are considered a result of CH_4 production below 50 cm but also due to a reduced diffusion through a layer of fine grained gytje situated between 55 and 60 cm. In the laboratory experiment, this gytje layer of reduced

Fig. 6. (a) O_2 (% air sat.) distribution in the peat column during a drainage experiment. *T*: time in minutes. WTD: water table depth. The images size is 6 × 8 cm. At T_0 the column was fully saturated with 5 cm aerated water above the soil surface and was drained to −40 cm. The white box indicates the area used in the areal integration of O_2 content during drainage. × signifies the depth of the MIMS orifice for CH_4 measurements. (b) O_2 contents (●) and CH_4 (×) concentrations measured during the drainage sequence. O_2 content were calculated as an average concentration in a 1 × 4 cm area between 3.5 and 4.5 cm depth from planar optode images. Error bars show ±1 SD from the mean. CH_4 concentrations are measured using MIMS at a fixed depth of 4 cm. Perforated vertical lines indicate when planar optode images in (a) were taken.

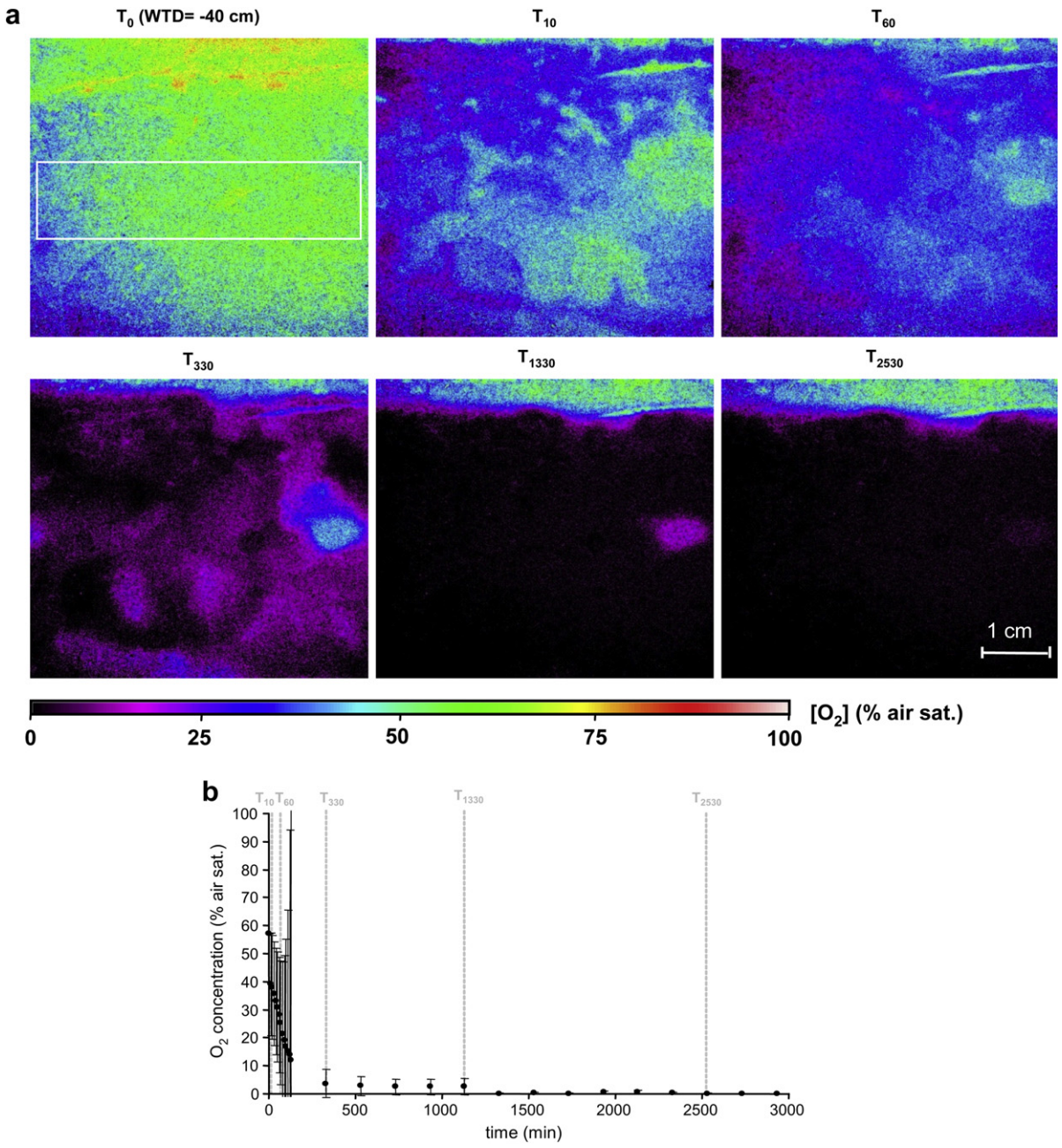

Fig. 7. (a) O_2 (% air sat.) distribution in a peat column during a water saturation experiment. *T*: time in minutes. WTD: water table depth. The images size is 6 × 7 cm. At T_0 the column was drained to −40 cm and was thereafter fully saturated with 5 cm aerated water above the soil surface. (b) Area-integrated O_2 (●) content measured during a drainage experiment. The O_2 content was calculated as an average in a 4 × 6 cm area between 2 and 6 cm depth from planar optode images. Error bars show ±1 SD from the mean. Perforated vertical lines indicate when planar optode images in (a) were taken.

diffusivity was not included. Furthermore, plant-mediated gas transport was not taken into account in our study as vegetation was not incorporated in our mesocosm experiments or static chamber plots. In the field, plant roots of *P. arundinacea* are known to facilitate transport of both O_2 downwards and CH_4 upwards (Laanbroek, 2010) thus influencing both O_2 and CH_4 concentrations. Future studies of such plant related gas exchange would also benefit from the planar optode methodology introduced in this study.

During fully saturated conditions in the peat mesocosm, highest CH_4 concentrations were observed around 5 cm depth below the soil surface decreasing towards −25 cm depth and thereafter increasing again with depth (Fig. 5a). The CH_4 concentration range measured in the mesocosm experiment corresponded well to field measurements and to previous studies of CH_4 concentrations measured in Swedish peat soil cores at 10 °C (Sheppard et al., 2006). NMR analyses showed that the surface peat deposits (0–5 cm) contained the largest amount of young and labile carbon and thus had the potential for the largest CH_4 production. In contrast to the non-vegetated laboratory mesocosm, the density of live roots in the top 20 cm of the soil was high. *P. arundinacea* is known to be able to transport O_2 to the root tips where it leaks out to the surrounding soil matrix creating a 0.1 mm aerobic layer around the roots (Edwards et al., 2006). Such rhizosphere oxygenation may explain the absence of high CH_4 concentrations in this layer with ample labile carbon in the field (Fig. 3), in contrast to higher near-surface CH_4 concentrations observed in the laboratory

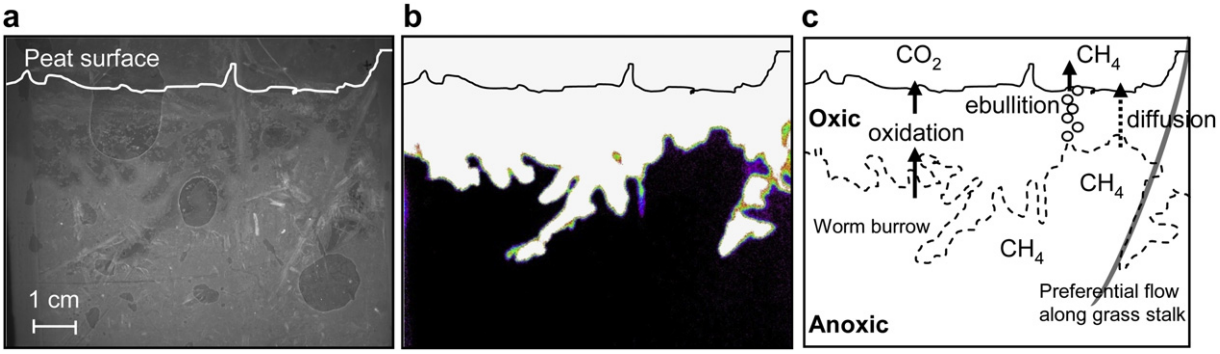

Fig. 8. (a) Planar optode b/w image of mesocosm peat profile at WTD − 4 cm. (b) Planar optode image of O_2 distribution in peat mesocosm profile at WTD − 4 cm. (c) Schematic image of soil heterogeneity, O_2 distribution, and fate of CH_4 produced in the anoxic zone.

mesocosm (Fig. 5a). This further limits the importance of ebullition under field conditions, particularly, as compared to laboratory conditions without plants.

Most known methanogens are neutrophilic, thus the near neutral pH of the peat soil should not limit CH_4 production. CH_4 concentrations increased at depths 25 cm below the soil surface due to reduced oxidation at depth. This is in agreement with observations of CH_4 ebullition events through the hole after profiling signifying a gas phase accumulation at depth.

MIMS profiles were made in different parts of the column to reduce effects of repeated profiles. This may be the reason for part of the large variability in CH_4 concentrations. Although the general trend in profiles was similar, CH_4 hotspots with concentrations up to 6 fold higher than the surrounding were noted in one profile.

4.3. Soil methane flux

Headspace measurements of CH_4 emissions from the water-logged peat soil in the mesocosm (0.2 mg CH_4-C m^{-2} d^{-1}) and in the field (2–17 mg CH_4-C m^{-2} d^{-1}) were very low in comparison to emissions reported from other studies of temperate wetlands (23–254 mg CH_4-C m^{-2} d^{-1}, Crill et al., 1988). Our low values could be due to enhanced oxidation of the CH_4 in the 5 cm overlaying oxygenated water column in the mesocosm (Bubier, 1995), but our field soil fluxes were also found to be in a similar range. One of the replicate mesocosms had a high emission rate during the measurement period (263 mg CH_4-C m^{-2} d^{-1}) which may be due to ebullition of free phase gas, commonly trapped beneath confining layers which may have escaped as a consequence of air mixing inducing a small pressure affect before the sampling (Whalen, 2005). Therefore this sample was omitted.

4.4. Oxygen and methane dynamics under changing water levels

Planar optode data underlined that the presence of small-scale structural heterogeneity in the soil must be considered in order to understand subsurface gas dynamics at the pedon scale during changes in water level. Mapping of two-dimensional O_2 contents with planar optodes enabled both a visualisation (Supporting information, Video 1) and a quantification of the role of heterogeneity in the O_2 distribution. Areal integration of O_2 measurements (4.5 cm^2) showed e.g. that the O_2 content above the water table after drainage can vary from 0 to 100% air saturation in periods up to several days after lowering the water level.

MIMS CH_4 concentration measurements were relatively stable at fully water-saturated conditions around 600 μM decreasing only slightly with increasing O_2 content ($y = -28x + 720$, $r^2 = 0.67$). As drainage continued, area-integration of O_2 measurements (4.5 cm^2) showed that below 30% air saturation, O_2 was not a limiting factor for the presence of CH_4 in the soil studied. This is due to both reduced CH_4 production in the limited anoxic zones and increased CH_4 oxidation, as oxic zones become more widespread resulting in a large surface area to volume ratio, enabling increased oxidation.

Under saturating conditions, water percolation was observed through macropores in the peat soil. Such macropores are the result of plant roots and activity of soil fauna (in this case earthworms, see Supporting information Videos 2 and 3). Moving earthworms in the soil create pathways. At first the O_2 content is lower around the worm potentially as a result of enhance diagenetic activity. From marine environments it is well described that burrow linings of infauna represent microbial hotspots of intensified mineralization activity (Aller and Aller, 1986; Jørgensen et al., 2005). However, burrows in the wetland subsequently act as macropores where fast response to changes in water and O_2 supply can be observed (Abe and Buck, 1985) as well as facilitating ebullition of gases. Macropores enable oxygenated water from precipitation to infiltrate faster and to displace trapped gas in the pore space.

Air displacement also resulted in a faster O_2 depletion rate at the start of saturation. In contrast, macropores can under field conditions also facilitate transport by capillary forces of reduced ground water up through the soil profile. However, this was not studied in this experiment.

After saturation, O_2 availability from the surface is reduced to the amount which diffuses through water and is released from roots. The planar optode image shows the oxygenated air is displaced by the water in the same macropores seen in the drainage sequence. An oxic soil aggregate was present up to 24 h after the saturation event illustrating that CH_4 oxidation can take place even in reduced bulk soil systems and that zones of lower O_2 consumption are present.

4.5. Limitations and future perspectives of planar optodes

It cannot be disregarded that all work with planar optodes potentially results in physical changes of the soil structure due to the effects of a Plexiglas wall as well as the wall presenting an area with potentially less friction for macrofauna burrowing, etc. Using planar optodes to evaluate structural changes under changing water levels may not reflect conditions in the soil interior. Compaction presents the largest challenge as the soil must be in direct contact with the planar optode in order for O_2 measurements to be reliable. However, in this study the effect is kept minimal as the soil was not dried for longer periods of time to avoid lateral soil compaction and to maintain a continuous soil contact with the wall.

In contrast to the temperature-controlled and non-vegetated conditions studied in the laboratory mesocosms, natural systems are very dynamic. Future studies including living *P. arundinacea* are important for assessing the linkage between plant-controlled O_2 transport to the rhizosphere as well as acting as CH_4 conduits from anoxic layers to the atmosphere. Radial O_2 loss from roots is of interest as it could increase CH_4 oxidation in an otherwise anoxic zone, reducing the amount of CH_4 reaching the aerenchyma. In contrast, root exudates produced are an important labile carbon source for CH_4 production possibly counteracting the increased oxidation in the root zone. The present study has proven that the planar optode setup is an effective method for assessing the O_2 distribution in wetlands and highlights the need for future studies of O_2 distribution in relation to greenhouse gas emissions (both CH_4 and N_2O) under natural vegetated conditions.

5. Conclusions

Wetland ecosystems exhibit a complex interaction of environmental parameters in the soil matrix. It has previously been difficult to visualize the heterogeneity of the peat structure and to link this heterogeneity to O_2 availability under fluctuating water levels. However, this study shows i) the potential of planar optodes for studies of O_2 dynamics controlled by soil structure and fluctuating water levels, ii) that small-scale soil heterogeneity resulting from macro-flora and macrofauna strongly affect the spatial distribution of O_2 availability in wetland soils under fluctuating water levels, and iii) that O_2 in turn controls the oxidation of CH_4 under aerobic conditions, and the distribution of anoxic zones where CH_4 can be produced.

The O_2 content above the water table after drainage was found to vary from 0 to 100% air saturation on the cm^2 scale. Oxic zones were observed below the water level and anoxic zones were observed above the water level in periods up to days after changes in water level. This visualisation and quantification of soil heterogeneity in relation to O_2 dynamics and changes in water level is important in the understanding of CH_4 consumption and transport, in wetland ecosystems with fluctuating water levels, both small scale (cm^2) and on an ecosystem level in a global change perspective.

Acknowledgements

This study was conducted within the framework of the project “Oxygen availability controlling the dynamics of buried organic carbon pools and greenhouse emissions” financed by the Danish National Research Council. Further financial support was supplied by the National Environmental Research Council (NERC) and the Commission for Scientific Research in Greenland. We wish to thank Ole Bennike (GEUS) and the AMS ^{14}C dating centre at Department of Physics and Astronomy, Aarhus University for help with ^{14}C dating and Heike Knicker, Lehrstuhl für Bodenkunde, Technische Universität München for help with solid-state ^{13}C NMR analyses. Special thanks to Lars Rickelt for constructing the planar optodes, technical assistance and for many valuable discussions. Thanks to Gry Lyngsie and Louise Langhorn for help with fieldwork, sample collection and laboratory analysis as well as Thomas Willumsen for MIMS calibration and help with intensive measurements.

Appendix. Supplementary information

Supplementary data associated with this article can be found in the online version at doi:10.1016/j.soilbio.2010.08.026.

References

Abe, A.S., Buck, N., 1985. Oxygen uptake of active and aestivating earthworm *Glossoscolex paulistus* (Oligochaeta, Glossosolecidae). Comparative Biochemistry and Physiology 81A (1), 63–66.

Aller, J.Y., Aller, R.C., 1986. Evidence for localized enhancement of biological activity associated with tube and burrow structures in deep-sea sediments at the HEBBLE site, western North Atlantic. Deep Sea Research 33, 755–790.

Bernstead, J., Lloyd, D., 1994. Direct mass spectrometric measurement of gases in peat cores. FEMS Microbiology and Ecology 13, 233–240.

Blossfeld, S., 2008. Plant Growth Dynamics in Relation to Soil Moisture, Oxygen Concentration and pH-value. Inaugural-Dissertation zur Erlang der Doktorgrades der Mathematisch-Naturwissenschaftlichen Fakultät der Heinrich-Heine Universität Dusseldorf (PhD thesis).

Bubier, J., 1995. The relationship of vegetation to methane emission and hydrochemical gradients in northern peatlands. The Journal of Ecology 83 (3), 403–420.

Christensen, C., 1981. Havniveauændringer 5500–2500 f.Kr. i Vedbækområdet, NØ-Sjælland. Dansk Geologisk Forening, Årsskrift for 1981, pp. 91–107 (in Danish).

Cook, P.L.M., Wenzhöfer, F., Glud, R.N., Janssen, F., Huettel, M., 2007. Benthic solute exchange and carbon mineralization in two shallow subtidal sandy sediments: impact of advective porewater exchange. Limnology and Oceanography 52, 1943–1963.

Couwenberg, J., 2009. Methane Emissions From Peat Soils (Organic Soils, Histosols). Facts, MRV-ability, Emission Factors. Greifswald University, Wetlands International, Ede.. www.wetlands.org.

Cowie, G., Lloyd, D., 1999. Membrane inlet ion trap measurement of dissolved gases in ecological samples. Journal of Microbiological Methods 35, 1–12.

Crill, P., Bartlett, K.B., Harriss, R.C., Gorham, E., Verry, E.S., Sebacher, D.I., Madzar, L., Sanner, W., 1988. Methane flux from Minnesota peatlands. Global Biogeochemical Cycles 2, 371–384.

Dedysh, S.N., 2002. Methanotrophic bacteria of acidic Sphagnum peat bogs. Microbiology 71 (6), 638–650.

Edwards, K.R., Cizkova, H., Zemanova, K., Santruckova, H., 2006. Plant growth and microbial processes in a constructed wetland planted with *Phalaris arundinacea*. Ecological Engineering 27, 153–165.

Fenchel, T., Glud, R.N., 2000. Benthic primary production and O_2-CO_2 dynamics in a shallow water sediment: spatial and temporal activity. Ophelia 53, 159–171.

Freeman, C., Lock, M.A., Reynolds, B., 1992. Fluxes of CO_2, CH_4 and N_2O from a Welsh peatland following simulation of water table draw-down: potential feedback to climatic change. Biogeochemistry 19 (1), 51–60.

Frediksen, M.S., Glud, R.N., 2006. Oxygen dynamics in the rhizosphere of *Zostera marina*: a two-dimensional planar optode study. Limnology and Oceanography 52, 1072–1083.

Glud, R.N., Ramsing, N.B., Gundersen, J.K., Klimant, I., 1996. A new tool for fine scale measurements of two-dimensional O_2 distribution in benthic communities. Marine Ecology Progress Series 140, 217–226.

Glud, R.N., Tengberg, A., Kühl, M., Hall, P.O.J., Klimant, I., 2001. An in situ instrument for planar O_2 optode measurements at benthic interfaces. Limnology and Oceanography 46, 2073–2080.

Holst, G., Kohls, O., Klimant, I., König, B., Kühl, M., Richter, T., 1998. A modular luminescence lifetime imaging system for mapping oxygen distribution in biological samples. Sensors and Actuators B 51, 163–170.

Holst, G., Franke, U., Grunwald, B., 2002. Transparent oxygen optodes in environmental applications at fine scale as measured by luminescence lifetime imaging. In: Proceedings of SPIE. International Society of Optical Engineering, Advanced Environmental Sensing Technology II, vol. 4576, pp. 138–148.

IPCC, 2007. Climate change 2007. The physical science basis. In: Solomon, S., Qin, D., Manning, M., Chen, Z., Marquis, M., Averyt, K.B., Tignor, M., Miller, H.L. (Eds.), Contribution of Working Group I to the Fourth Assessment. Report of the Intergovernmental Panel on Climate Change. Cambridge University Press, Cambridge, United Kingdom and New York, NY, USA, p. 996.

Jensen, S.I., Kühl, M., Glud, R.N., Jørgensen, L.B., Primé, A., 2005. Oxygen microzones and radial oxygen loss from roots of *Zostera marina*. Marine Ecology Progress Series 293, 49–58.

Jobbagy, E.G., Jackson, R.B., 2000. The vertical distribution of soil organic carbon and its relation to climate and vegetation. Ecological Applications 10 (2), 423–436.

Jørgensen, B.B., Glud, R.N., Holby, O., 2005. Oxygen distribution and bioirrigation in Arctic fjord sediments Svalbard, Barents Sea. Marine Ecology Progress Series 292, 85–95.

Kammann, C., Grunhage, L., Jager, H.-J., 2001. A new sampling technique to monitor concentrations of CH_4, N_2O and CO_2 in air at well-defined depths in soils with varied water potential. European Journal of Soil Science 52, 297–303.

Kiem, R., Knicker, H., Körschens, M., Kögel-Knabner, I., 2000. Refractory organic carbon in C-depleted arable soils as studied by ^{13}C NMR spectroscopy and carbohydrate analysis. Organic Geochemistry 31, 655–668.

Klimant, I., Meyer, V., Kühl, M., 1995. Fiber-optic oxygen microsensors, a new tool in aquatic biology. Limnology and Oceanography 40, 1159–1165.

Kühl, M., 2005. Optical microsensors for analysis of microbial communities. Methods in Enzymology 397, 166–199.

Kühl, M., Polerecky, L., 2008. Functional and structural imaging of phototrophic microbial communities and symbioses. Aquatic Microbial Ecology 53, 99–118.

Laanbroek, H., 2010. Methane emission from natural wetlands: interplay between emergent macrophytes and soil microbial processes. A mini-review. Annals of Botany 105, 141–153.

Lai, D.Y.F., 2009. Methane dynamics in Northern Peatlands: a review. Pedosphere 19 (4), 409–421.
Landström, S., Lomakka, L., Andersson, S., 1996. Harvest in spring improves yield and quality of reed canary grass as a bioenergy crop. Biomass and Bioenergy 11 (4), 333–341.
Lauritsen, F.R., Choudhury, T.K., Dejarme, L.E., Cooks, R.G., 1992. Microporous membrane introduction mass spectrometry with solvent chemical ionization and glow discharge for the direct detection of volatile organic compounds in aqueous solution. Analytica Chimica Acta 266, 1–12.
Lloyd, D., Thomas, K., Price, D., O'Neil, B., Oliver, K., Williams, T.N., 1996. A membrane-inlet mass spectrometer miniprobe for the direct simultaneous measurement of multiple gas species with special resolution of 1 mm. Journal of Microbiological Methods 25, 145–151.
Le Mer, J., Roger, P., 2001. Production, oxidation, emission and consumption of methane by soils: a review. European Journal of Soil Science 37, 25–50.
Öquist, M., Sundh, I., 1998. Effects of a transient oxic period on mineralization of organic matter to CH_4 and CO_2 in anoxic peat incubations. Geomicrobiology 15, 325–333.
Precht, E., Franke, U., Polerecky, L., Huettel, M., 2004. Oxygen dynamics in permeable sediments with a wave-driven pore water exchange. Limnology and Oceanography 49, 693–705.
Rickelt, L.F., Askaer, L., Elberling, B., Glud, R.N., Kühl, M. A sensor array for long term in situ measurements of O_2 and temperature dynamics in soil and sediment, in preparation.
Roulet, N.T., Ash, R., Quinton, W., 1993. Methane flux from drained northern peatlands: effect of a persistent water table lowering on flux. Global Biogeochemical Cycles 7, 749–769.
Rysgaard, S., Glud, R.N., Sejr, M.K., Blicher, M.E., Staahl, H.J., 2008. Denitrification activity and oxygen dynamics in Arctic sea-ice. Polar Biology 31, 527–537.
Segers, R., 1998. Methane production and methane consumption: a review of processes underlying wetland methane fluxes. Biogeochemistry 41, 23–51.
Schaefer, J., Stejskal, E.O., 1976. Carbon-13 nuclear magnetic resonance of polymers spinning at magic angle. Journal of American Chemical Society 98, 1031–1032.
Sheppard, S.K., Lloyd, D., 2002. Direct mass spectrometric measurement of gases in soil monoliths. Journal of Microbiological Methods 50, 175–188.
Sheppard, S.K., Beckmann, M., Loyd, D., 2006. The effect of temperature on methane dynamics in soil and peat cores: calculations from membrane inlet mass spectrometry. Canadian Journal of Soil Science 87 (1), 11–22.
Thomas, K.L., Lloyd, D., 1995. Measurement of denitrification in estuarine sediment using membrane inlet mass spectrometry. FEMS Microbiology and Ecology 16, 103–114.
Thorstenson, D.C., Pollock, D.W., 1989. Gas transport in unsaturated zones: multicomponent systems and the adequacy of Fick's laws. Water Resources Research 25, 477–507.
Wachinger, G., Fiedler, S., Zepp, K., Gattinger, A., Sommer, M., Roth, K., 2000. Variability of soil methane production on the micro-scale: spatial association with hot spots of organic material and archaeal populations. Soil Biology & Biochemistry 32, 1121–1130.
Watson, A., Stephen, K.D., Nedwell, D.B., Arah, J.R.M., 1997. Oxidation of methane in peat: kinetics of CH_4 and O_2 removal and the role of plant roots. Soil Biology & Biochemistry 29 (8), 1257–1267.
Weiss, R., Alm, J., Laiho, R., Jukka, L., 1998. Modelling moisture retention in peat soils. Soil Society of America Journal 62 (2), 305–313.
Wenzhöfer, F., Glud, R.N., 2004. Small-scale spatial and temporal variability in benthic O_2 dynamics of coastal sediments: impact of fauna activity. Limnology and Oceanography 49, 1471–1481.
Whalen, S.C., 2005. Biogeochemistry of methane exchange between natural wetlands and the atmosphere. Environmental Engineering Science 22, 73–94.
Wilke, C.R., Chang, P., 1955. Correlation of diffusion coefficients in dilute solutions. American Institute of Chemical Engineers Journal 1 (2), 264–270.
Witkowska-Walczak, B., Bieganowski, A., Rovdan, E., 2002. Water-air properties in peat, sand and their mixtures. International Agrophysics 16, 313–318.